https://doi.org/10.6113/TKPE.2020.25.5.358

계통연계 인버터를 위한 디지털 록인 앰프 기반의 새로운 고조파 보상법

사기르 아민[1], 무하마드 노만 아슈라프[1], 최우진†

A Novel Digital Lock-In Amplifier Based Harmonics Compensation Method for the Grid Connected Inverter Systems

Saghir Amin[1], Muhammad Noman Ashraf[1], and Woojin Choi†

Abstract

Grid-connected inverters (GCIs) based on renewable energy sources play an important role in enhancing the sustainability of a society. Harmonic standards, such as IEEE 519 and P1547, which require the total harmonic distortion (THD) of the output current to be less than 5%, should be satisfied when GCIs are connected to a grid. However, achieving a current THD of less than 5% is difficult for GCIs with an output filter under a distorted grid condition. In this study, a novel harmonic compensation method that uses a digital lock-in amplifier (DLA) is proposed to eliminate harmonics effectively at the output of GCIs. Accurate information regarding harmonics can be obtained due to the outstanding performance of DLA, and such information is used to eliminate harmonics with a simple proportional - integral controller in a feedforward manner. The validity of the proposed method is verified through experiments with a 5 kW single-phase GCI connected to a real grid.

Key words: PV (Single Stage Photovoltaic System), MPPT (Maximum Power Point Tracking), Harmonic compensation method

1. Introduction

Photovoltaic energy has become one of the most popular sustainable energy sources nowadays. Due to the continuous cost reduction and government incentives, the installation of grid-integrated PV system has grown rapidly in the past few years[1].

In the Grid Connected Inverters (GCIs) the grid current control is an essential part. There are two most common methods to control the grid current; one is the Stationary Reference Frame (SRF) control and the other is the Rotatory Reference Frame (RRF) control[2],[3]. In the RRF controllers, simple PI control can provide a good control performance since the transformation turns AC quantities into DC quantities. The design process of the PI controller is simple, and it provides satisfactory dynamic and steady-state performance. Since the system variables are converted to DC quantities, the control loop has no dependence on the system frequency. In addition, this scheme provides independent regulation for active and reactive power by the simple adjustment of the d and q axis current[4].

The simple PI controller for the current control in RRF is not robust in compensating the low order harmonic components and it can hardly satisfy the harmonic standard such as IEEE 519 and P1547[5]. In order to fulfill the international harmonic standards and meet the required THD value for the inverter output under the distorted grid condition, the use of harmonic controller is essential.

Total Harmonic Distortion (THD) is a measure of

Paper number: TKPE-2020-25-5-4
Print ISSN: 1229-2214 Online ISSN: 2288-6281
† Corresponding author: cwj777@ssu.ac.kr, Dept. of Electrical Eng., Soongsil University
Tel: +82-2-820-0652 Fax: +82-2-817-7961
[1] Dept. of Electrical Eng., Soongsil University
Manuscript received Oct. 28, 2019; revised Dec. 3, 2019; accepted Jan. 22, 2020
— 본 논문은 2019년 전력전자학술대회 태양광논문상 수상논문임

all of the harmonics present in a current or voltage waveform with respect to the fundamental frequency component. Generally, non-ideal behavior of the switches used in GCIs leads to an increasing THD at the inverter output. The output of the inverter isdistorted by three main factors. The first is the device turn-on/off delays, conduction voltage drops across the power switches and the dead-band of PWM effects to prevent the shoot-through fault between the lower and upper switches. The second is the dc-offset and scaling error in the current and voltage sensing circuit. The third is the harmonics that are already present in the grid due to the extensive use of non-linear loads nowadays. The harmonics present in the grid also induces low order harmonics during the closed-loop control operation of the GCIs[6]. In addition, the LCL output filters are preferred to reduce the switching frequency harmonics in GCIs due to their excellent high-frequency attenuation performance. However, it dramatically increases the susceptibility to low-order current distortions because of its lower inductance value as compared to L or LC filter[7]. Therefore, instead of increasing the inductance of the output filter, hence the cost and the volume, it is preferred to use harmonic compensation methods.

To avoid the adverse effects of GCIs on the grid power quality, their minimum output quality is suggested by the grid standards such as IEEE 1547, which specifies the limits for individual harmonics[8]. However, the conventional RRF current controllers have some limitations as followings. In the conventional methods the harmonic compensators are connected in parallel to the fundamental current controller. This approach is widely used, and several variations can be found in the literature[9]-[11].

The Proportional Resonant (PR)[9], the Second Order Generalized Integrator (SOGI)[10] and the Repetitive Controller (RC)[11] are employed in parallel with the current controller (PI) in the d and q axis, respectively, to detect a certain harmonic and compensate it in a feedforward manner. Although this control method is effective in harmonic rejection, one of the disadvantage of this method is that four compensators are required to eliminate a certain harmonic. Since a harmonic component in the SRF appears as two different frequency components in the RRF, it should be compensated for both the d and q axis. Another disadvantage is that the OSGs are generated by the SOGI, which is composed of low pass filters and a band pass filter. As a result, it is inherently impossible to extract the accurate information about the harmonic components due to the attenuation of the filter. Thus, these harmonic controllers are not able to perfectly compensate for the harmonics. The harmonic compensators with proportional-resonant controllers are very sensitive to frequency variations when their quality factor is selected to be high to provide a high gain for a certain harmonic since the gain would be significantly reduced by a slight change in the resonant poles due to the error caused by the discretization[12]. If the controller is designed with a lower quality factor to increase the robustness towards frequency variations, undesirable frequency components may be amplified, leading to a lower output quality of the GCIs[13]. In [10], a SOGI is added in parallel with the current regulator for both the D and Q axis. However, since a low pass filter and a band pass filter are included in the SOGI block, it makes the control more complicated and increases the computational burden.

In this paper a novel harmonic compensation method by using a Digital Lock-In Amplifier (DLA) is proposed to overcome the limitations of conventional methods. Due to the outstanding performance of the DLA to detect a certain frequency component under the extremely noisy environment it is possible to extract the amplitude and phase information of a certain harmonic component with high accuracy. The extracted harmonic information is used to reconstruct the harmonic and used to compensate it through the PI controller. The detail design procedure for the proposed method with DLA is presented after describing the current control and the validity of the proposed method is verified through the experiments with a 5kW GCI working for a PV system. The Maximum Power Point Tracking (MPPT) for the PV system is implemented with the help of Ripple Correlation correction (RCC) method.

2. Grid Current Control of the Single Phase GCI for PV Power Generation System

Fig. 1 shows the general block diagram of a single-phase grid-connected PV inverter controlled in DQ frame, where a single-phase H-bridge inverter injects the PV power to the grid through a passive LCL filter. The grid voltage and current are fed back

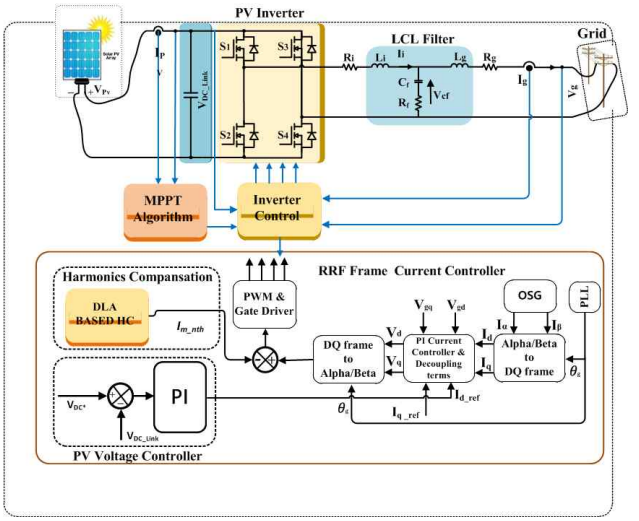

Fig. 1. Proposed single-phase PV system with RRF based current controller and harmonic compensator using DLA.

to the controller for the control. The controller injects a sinusoidal current satisfying the power quality and the dynamic performance. In the Rotatory Reference Frame (RRF) controllers, since the transformation turns ac quantities into dc quantities, the PI controller can provide a good control performance. Though the design process of the PI controller is simple, it can provide a satisfactory dynamic and steady-state performance. In addition, as the system variables are converted to dc quantities, the control loop has no dependence on the system frequency. It is also possible to provide the independent regulation for active and reactive power by the simple adjustment of the d and q axis current. Even though RRF based current controller have higher computational burden due to Park Transformation and the inverse Park Transformation than that of the Stationary Reference Frame (SRF) based control, its implementation is not difficult thanks to the availability of the high performance DSP with lower cost in these days.

As shown in Fig.1, the current controller requires an orthogonal Signal Generator (OSG) block to generate the α and β axis components of the grid current. In this research the Second-Order Generalized Integrator (SOGI) is used as OSG as it can generate the OSG signals perfectly due to its good attenuation or filtering capability over the harmonic components[14]. The Phase-Locked-Loop (PLL) is used in this scheme to synchronize the controller to the grid voltage. Fig.2 shows the conventional current controller on the RRF. The controller consists of two PI controllers, the decoupling terms and the feed

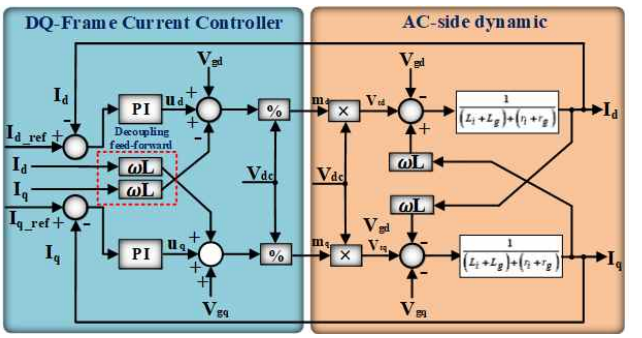

Fig. 2. Block diagram of the conventional current controller on the RRF.

forward terms in both d and q axes which is similar to the three-phase d-q frame current controllers[15].

From Fig. 2, the dynamic equation for the ac side can be expressed as Eq. (1).

$$\begin{aligned} V_{inv} &= R_i I_i + sL_i I_i + V_{cf} \\ V_{cf} &= R_g I_g + sL_g I_g + V_g \\ I_i &= I_g + C_f \frac{V_{cf}}{s} \end{aligned} \tag{1}$$

Where, V_{inv}, V_{cf}, V_g, I_i and I_g is the inverter terminal voltage, the capacitor voltage, the utility grid voltage, the converter-side current and the grid current, respectively. If the effect of the small capacitor in the LCL filter is neglected, then the design of the current control is the same as is the case with VSI with L filter. Thus, in the α-β frame, Eq. (1) can be simplified to Eq.(a)2).

$$\begin{aligned} V_{inv\_\alpha} &= (R_i + R_g) I_\alpha + s(L_i + L_g) I_\alpha + V_{g\_\alpha} \\ V_{inv\_\beta} &= (R_i + R_g) I_\beta + s(L_i + L_g) I_\beta + V_{g\_\beta} \end{aligned} \tag{2}$$

Furthermore, Eq. (2) needs to be transformed from SRF to RRF by using the relationship $x_{dq}=x_{dq}e^{-jwt}$. Therefore, the dynamic equation of the ac-side variable in the RRF (dq frame) can be derived as Eq. (3).

$$\begin{aligned} V_{inv\_d} &= (R_i + R_g) I_d + s(L_i + L_g) I_d \\ &\quad - \omega_{ff}(L_i + L_g) I_q + V_{g\_d} \\ V_{inv\_q} &= (R_i + R_g) I_q + s(L_i + L_g) I_q \\ &\quad + \omega_{ff}(L_i + L_g) I_q + V_{g\_q} \end{aligned} \tag{3}$$

As shown in Eq. (3) and Fig. 2 there are cross couple terms and it should be compensated. In order to achieve a decoupling control of I_d and I_q, the inverter terminal voltage should be controlled as followings.

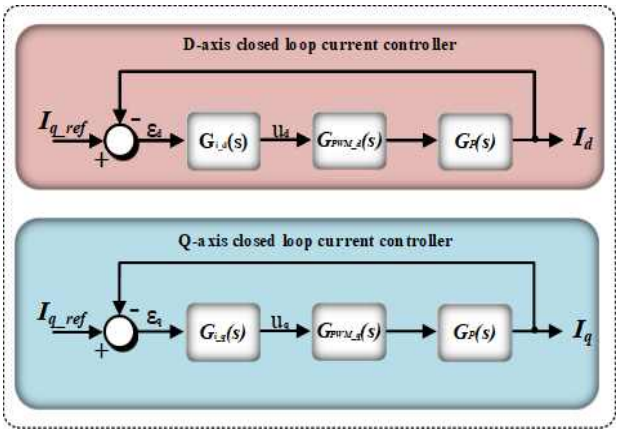

Fig. 3. Simplified block diagram of the current controller.

$$V_{inv\_d} = u_d - \omega_{ff}(L_i + L_g)I_q + V_{g\_d}$$
$$V_{inv\_q} = u_q - \omega_{ff}(L_i + L_g)I_d + V_{g\_q} \quad (4)$$

Where u_d and u_q is the control signal of the d and q axis in the RRF, respectively. By using Eq. (3) and Eq. (4), Eq. (5) can be derived.

$$u_d = (R_i + R_g)I_d + s(L_i + L_g)I_d$$
$$u_q = (R_i + R_g)I_q + s(L_i + L_g)I_q \quad (5)$$

Eq. (5) is the first order linear equation with two decoupled terms. Based on Eq. (5), I_d and I_q can be controlled by u_d and u_q, respectively. Fig. 2 shows a block diagram of the d and q axis current controller of the single-phase inverter, where u_d and u_q is the output of each PI current controller, respectively. In order to cancel the effect of decoupling terms and the grid voltage term present in the plant, these terms should be added to the current controller to be canceled each other. Therefore the current controller in Fig. 2 can be simplified to the one as shown in Fig. 3.

One advantage of DQ current controller is that both d and q axis current-control loops are identical as shown in Fig. 3. Therefore, the compensator at each axis is the same. The RRF current control structure, usually requires simple PI controllers due to its satisfactory dynamic performance and zero steady state error when regulating dc components. In Fig. 3 the $G_P(s)$ is the representation of the plant shown in Eq. (6) and $G_{PWM}(s)$ is the transfer function of the PWM unit in the S-domain, which comprises of a zero-order holder and a computation delay as Eq. (6) and Eq. (7).

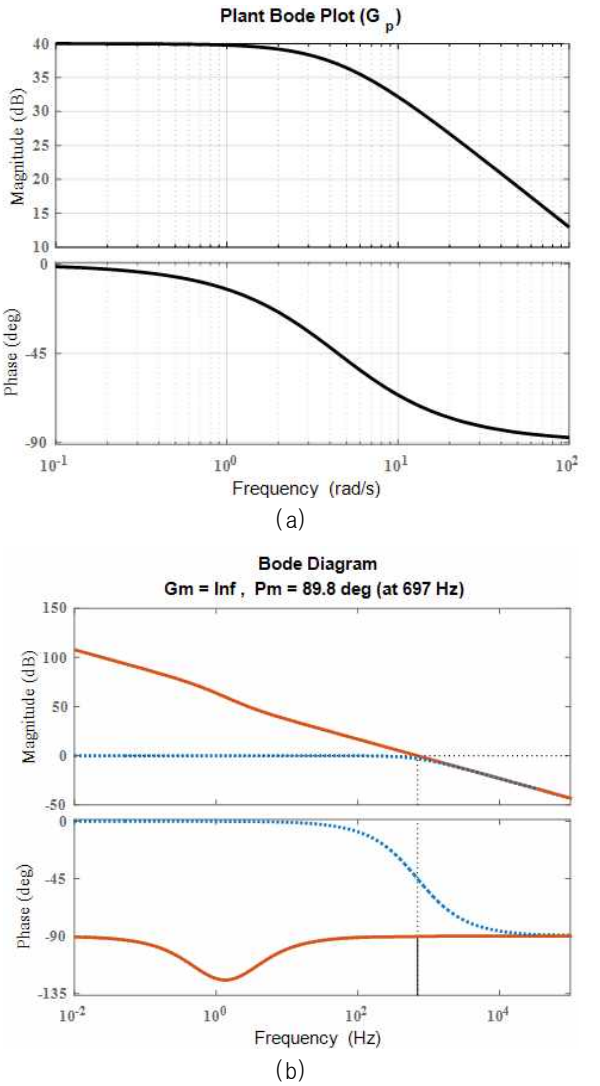

Fig. 4. Bode Plot. (a) Plant transfer function, (b) Loop gain and close loop transfer function.

$$G_P(s) = \frac{1}{(L_i + L_g) + (r_i + r_g)} \quad (6)$$

$$G_{PWM}(s) = \frac{e^{-T_s s}(1 - e^{-T_s s})}{T_s s} \approx \frac{1 - 0.5T_s s}{(1 + 0.5T_s s)^2} \quad (7)$$

Where T_s is the sampling time. From Fig. 3 the loop gain for of the whole system can be derived as Eq. (8).

$$G_{ol}(s) = G_i(s) * G_{PWM}(s) * G_P(s) \quad (8)$$

The frequency domain analysis of the plant can be performed by using Eq. (8) and the Bode diagrams of the loop gain can be plotted as shown in Fig. 4. When the current control loop is designed, it is desirable to maximize the bandwidth of the current controller by using a higher K_p so as to achieve the

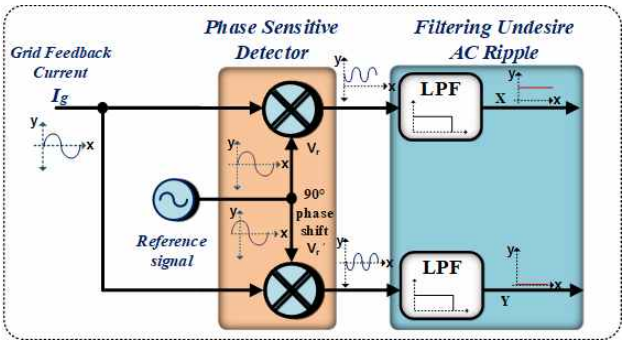

Fig. 5. Block diagram of the digital lock-in amplifier (DLA).

perfect reference tracking performance at all input frequencies, a faster dynamic response and the complete blocking of the disturbance input. However, a high gain can degrade the control loop stability in the actual implementation. They are in a trade-off relationship in between the bandwidth and the stability of the system.

By using MATLAB, the controller can be designed without difficulty. The bode plot of the loop gain $G_{ol}(s)$ is shown in Fig. 4(b). The parameters for the PI controller is obtained as K_p = 9.85 and K_i =157.7 The bandwidth of the current controller is 697Hz and the phase margin is 89.8 degrees.

3. Application of the Digital Lock-In Amplifier to Detect the Harmonics

It was already mentioned earlier that the main reason for the incomplete harmonic compensation of the previous methods can be attributed to inaccurate harmonic detection. In this paper a Digital Lock-in Amplifier (DLA) based harmonic detection and elimination method is proposed. In this chapter a DLA based harmonic detection and compensation method is presented and the design procedure is detailed. The block diagram of the Digital Lock-in Amplifier (DLA) and the proposed harmonic compensation method is shown in Fig. 5 and Fig. 6, respectively.

In the proposed method, the fundamental component of the grid current is regulated on the RRF with a simple PI controller. Meanwhile, individual harmonic is detected by means of DLA at its own frequency frame and compensated in a feedforward manner.

A block diagram of the DLA is shown in Fig. 5. In order to capture a certain frequency component a reference signal V_r and its orthogonal signal V_r' are generated and multiplied by the input signal V_s. This process is called Phase Sensitive Detection (PSD). Through the PSD process all the frequency components other than the reference frequency are rejected and only a signal with the same frequency as the reference signal remains. To show the effectiveness of the DLA the general equations to describe its principle are as follows. The input signal, reference signal and its orthogonal signal can be expressed by Eqs. (9)-(10) and (11).

$$V_s = V_m \sin(\omega_s t + \theta_s) \tag{9}$$

$$V_r = \sin(\omega_r t + \theta_r) \tag{10}$$

$$V_r' = \sin(\omega_r t + \theta_r) \tag{11}$$

When the reference signal and its orthogonal signal are multiplied to the input signal, the output of the PSD can be derived as Eqs. (12)-(13).

$$x' = \frac{V_m}{2}\begin{pmatrix}\cos((\omega_s-\omega_r)t+(\theta_s-\theta_r)) \\ -\cos((\omega_s+\omega_r)t+(\theta_s+\theta_r))\end{pmatrix} \tag{12}$$

$$y' = \frac{V_m}{2}\begin{pmatrix}\sin((\omega_s+\omega_r)t+(\theta_s+\theta_r)) \\ +\sin((\omega_s-\omega_r)t+(\theta_s-\theta_r))\end{pmatrix} \tag{13}$$

The PSD outputs are two AC signals, one is at the difference frequency of $(\omega_s-\omega_r)$ and the other is at the sum frequency $(\omega_s+\omega_r)$. From Eqs. (12)-(13), it is possible to extract the amplitude and phase information of the input signal if $\omega_s \approx \omega_r$. In order to obtain pure DC signals from the PSD output, it is further processed through a LPF to get only DC values.

4. Proposed Harmonic Compensation Method with DLA

In this section the harmonic detection process using a DLA (Fig. 6) is explained in detail. It is assumed that the grid current is distorted and it has odd harmonic components as shown in Eq. (14).

$$I_g = I_{amp}\begin{pmatrix}\sin(\omega_g t+\theta_g)+m_{3h}\sin(3\omega_g t+3\theta_g)+ \\ m_{5h}\sin(5\omega_g t+5\theta_g+... \\ +m_{nh}\sin(n\omega_g t+n\theta_g)\end{pmatrix} \tag{14}$$

Where I_{amp} represents the magnitude of the fundamental current, m_{nh} represents the amplitude of the harmonics in the feedback current, and “n”

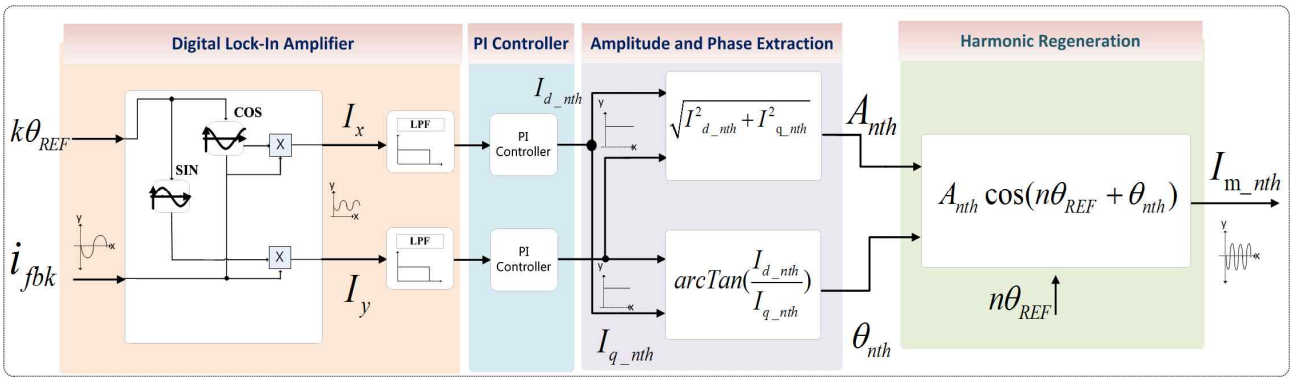

Fig. 6. Block diagram of the proposed harmonics compensation by using Digital Lock-in Amplifier (DLA).

represents the order of the harmonics. In order to detect the harmonic components, the reference and its orthogonal signal, which has a unity amplitude and an arbitrary theta at the harmonic frequency, need to be generated by a DSP as shown in (15).

$$\begin{aligned} I_{nh_{ref}} &= \sin(k\omega_{ref}t + k\theta_{ref}) \\ I_{nh'_{ref}} &= \cos(k\omega_{ref}t + k\theta_{ref}) \end{aligned} \tag{15}$$

Where "k" represents the order of the reference signal. The reference signals are multiplied by the grid current, which can be expressed by (16).

$$\begin{aligned} I_{\alpha_{nh}} &= I_g^* I_{nh_{ref}} = I_g^* \sin(k\omega_{ref}t + k\theta_{ref}) \\ I_{\beta_{nh}} &= I_g^* I_{nh'_{ref}} = I_g^* \sin(k\omega_{ref}t + k\theta_{ref}) \end{aligned} \tag{16}$$

Eqs. (17) and (18) can be derived using Eqs. (12), (13) and (16) as follows.

$$I_{\alpha_{nh}} = \frac{I_{amp}}{2}\left[\sum_{\substack{n=1,3,5..\\k=3,5...}} m_{nh}\begin{pmatrix}\cos\begin{pmatrix}(k\omega_{ref}-n\omega_g)t\\+(k\theta_{ref}-n\theta_g)\end{pmatrix}\\-\cos\begin{pmatrix}(k\omega_{ref}-n\omega_g)t\\+(k\theta_{ref}-n\theta_g)\end{pmatrix}\end{pmatrix}\right] \tag{17}$$

$$I_{\beta_{nh}} = \frac{I_{amp}}{2}\left[\sum_{\substack{n=1,3,5..\\k=3,5...}} m_{nh}\begin{pmatrix}\sin\begin{pmatrix}(k\omega_{ref}+n\omega_g)t\\+(k\theta_{ref}+n\theta_g)\end{pmatrix}\\+\sin\begin{pmatrix}(k\omega_{ref}-n\omega_g)t\\+(k\theta_{ref}-n\theta_g)\end{pmatrix}\end{pmatrix}\right] \tag{18}$$

From Eqs. (17) and (18) the phase and amplitude can be extracted if $k\omega_{ref} \approx n\omega_g$. The sub harmonic components, which are superimposed on a DC value can be eliminated by employing LPFs. The transfer function of an LPF used can be expressed as follows.

$$G_{LPF}(s) = \left(\frac{\omega_c}{s+\omega_c}\right)^n \tag{19}$$

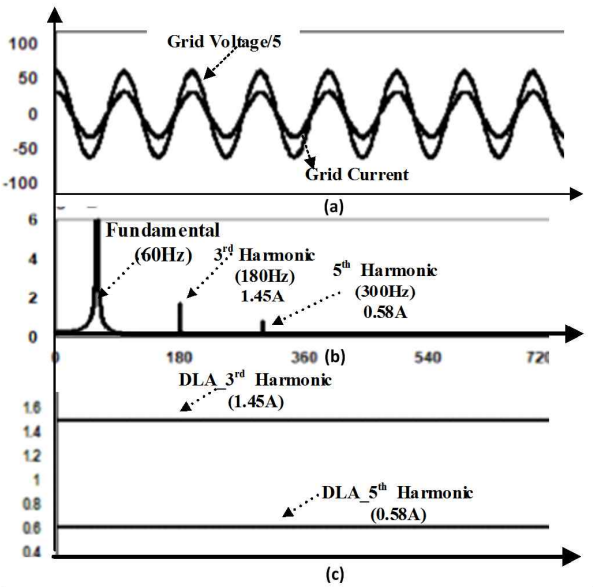

Fig. 7. Simulation results. (a) Grid current and voltage waveforms, (b) FFT result of the output current at 5 kW, (c) The detected 3rd and 5th harmonic amplitudes by the DLA.

Where n is the order of the LPF. In order to obtain accurate DC values that contain the amplitude and phase information of a certain harmonic component, the order of the LPF and its cut off frequency need to be selected carefully. It can be noted from Eqs. (17) and (18) that the lowest AC component is 120 Hz when the 3rd harmonic is compensated. Meanwhile, in case of 5th harmonic compensation, the lowest AC component is 240 Hz. Therefore, the LPF needs to be designed to sufficiently attenuate the 120 Hz and 240 Hz ripples.

In order to show the effectiveness of the DLA in detecting harmonics, the grid current is passed through the DLA to obtain the amplitudes of the 3rd and 5th harmonic components. Fig. 7(a) and (b) show the grid current with 3rd and 5th harmonic components and its FFT results, respectively. Fig. 7(c) shows

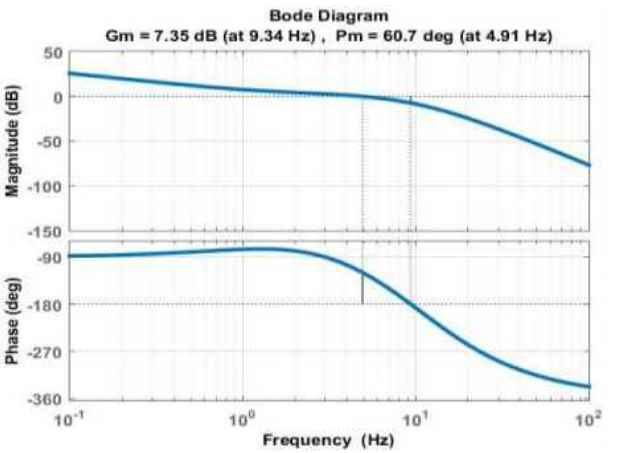

(a)

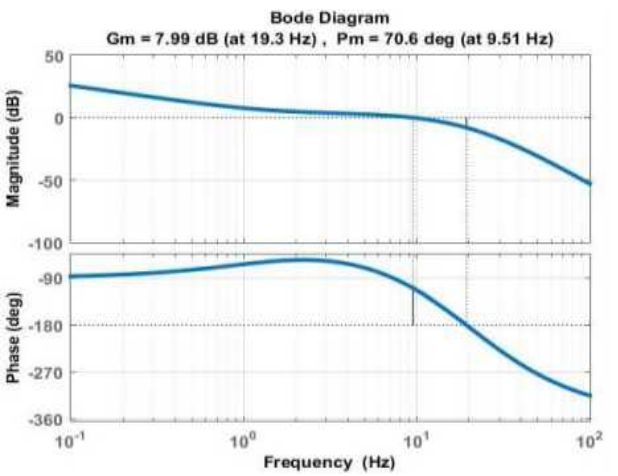

(b)

Fig. 8. Bode plot of the open loop gain. (a) $G_{ol3h}(s)$ for 3rd harmonic compensator, (b) $G_{ol5h}(s)$ for 5th harmonic compensator.

the amplitudes of the harmonics detected by the DLA. It can be noticed that the amplitudes of the harmonics are exactly the same as the FFT results, which are 1.45A and 0.58A for the 3rd and 5th harmonics, respectively.

The extracted magnitude and phase information of a certain harmonic component are used to reconstruct the harmonic. Then it is fed to a simple PI controller to compensate it by the negative feedback.

Since the magnitude and phase information of the harmonic in the proposed method is a DC value, the harmonic compensation can be performed with a simple PI controller. The open loop gain for the harmonic compensation loop can be expressed as in Eq. (20).

$$G_{ol_{nh}}(s) = LPF \times PI = \left(\frac{\omega_c}{s+\omega_c}\right)^n \times \left(\frac{k_p s + k_i}{s}\right) \quad (20)$$

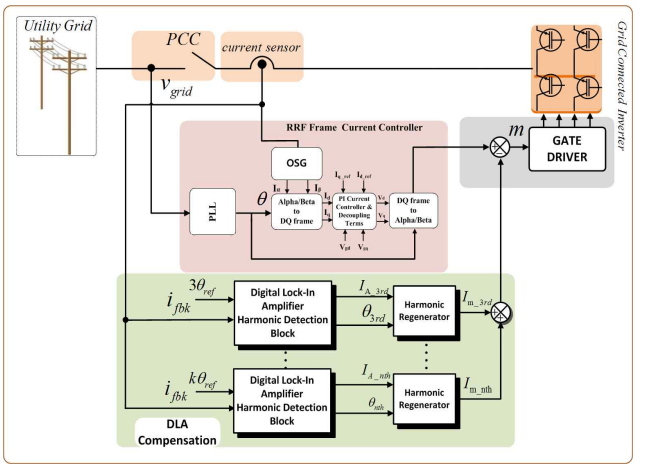

Fig. 9. Block diagram of the proposed DLA based harmonic compensation method.

To achieve effective harmonic compensation, the bandwidth of the PI controller should be less than the cut-off frequency of the LPF. A higher bandwidth selection for the PI controller may cause the harmonic compensation loop to become unstable. Bode plots of the open-loop gains of the 3rd and 5th harmonic controllers are chosen to be 1.489 and 12.07. To ensure the stability of the system, the phase margins for the 3rd and the 5th harmonic compensator are designed to be 60.7 degrees at 4.91 Hz and 70.6 degrees at 9.5 Hz, respectively, as shown in Fig. 8.

As previously explained, the harmonic are detected through the DLA and regulated by a PI controller. The harmonic can be simply reconstructed by using its amplitude and phase information detected by the DLA as expressed in Eq. (21).

$$m_{\alpha nh} = A_{nh}\cos(k\theta_{ref} + \theta_{nh}) \quad (21)$$

Where $m_{\alpha nh}$ is the reconstructed harmonic, A_{nh} is the amplitude of the harmonic component after the harmonic compensator, and θ_{nh} is the phase difference between the harmonic component and the reference signal. After the LPF, all of the residual ripples are removed except for the zero frequency DC values representing the amplitude and phase information of the detected harmonics. The amplitude and phase information of a certain harmonic can be computed as follows.

$$I_{dnh'} = \frac{I_{amp} * m_{nh}\left[\cos((k\omega_{ref} - n\omega_g)t + (k\theta_{ref} - n\theta_g))\right]}{2}$$
$$I_{qnh'} = \frac{I_{amp} * m_{nh}\left[\sin((k\omega_{ref} - n\omega_g)t + (k\theta_{ref} - n\theta_g))\right]}{2} \quad (22)$$

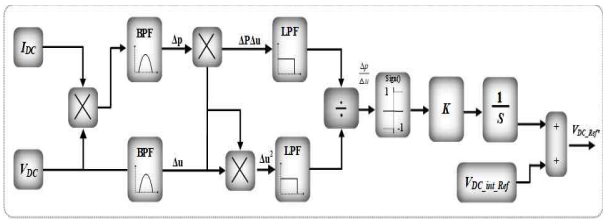

Fig. 10. Block diagram representation of RCC based MPPT algorithm.

$$A_{nh} = \sqrt{(I_{dnh'})^2 + (I_{qnh'})^2} \tag{23}$$

$$\theta_{nh} = \tan^{-1}\left(\frac{I_{qnh'}}{I_{dnh'}}\right) \tag{24}$$

Then the harmonic can be compensated in a feed forward manner by subtracting the reconstructed signal from the output of fundamental current controller as shown in Fig 9.

5. Maximum Power Point Tracking Algorithm

The objective of any Maximum power point tracking (MPPT) algorithm is to extract the maximum power from the PV modules. Mostly, the condition $\partial p/\partial v = 0$ is adopted to locate this operating point at the maximum power point (MPP). Number of MPPT methods have been proposed for maximum power tracking such as Perturb and Observe (P&O), Hill Climbing, Incremental Conductance, Fuzzy Logic control, Fractional open-circuit voltage control, Fractional short-circuit current control, Neural network, Ripple Correlation Control (RCC) and others. These methods differ in complexity, hardware, speed of convergence, sensors required, cost, range of effectiveness and other aspects.

5.1 Block diagram and convergence analysis

Fig. 10 shows the RCC-MPPT technique and it is the one which has the following advantages such as parameter-insensitivity, very fast convergence to reach MPP, simple and straightforward circuit implementation and well-explained theoretical analysis.

In RCC-MPPT, low frequency component is the mandatory component for tracking MPP. Hence, in most of the cases the low frequency component is injected from outside. In this approach instead of feeding the plant with sinusoidal probing signals, the control input is obtained by using the low frequency

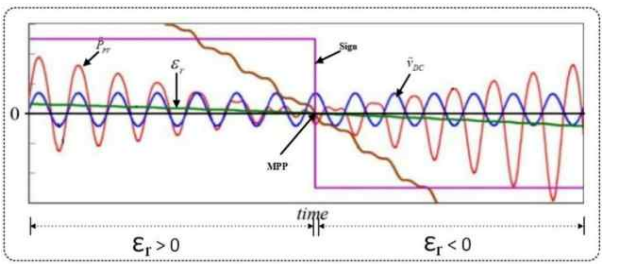

Fig. 11. Behavior of different signals at different power points.

component induced by the inverter at the PV side. Therefore, there is no need to generate the low frequency perturbation by the controller. This low frequency must be extracted by means of a separate filter. A band-pass filter is used to replace the high-pass filter as it is typically used in the RCC-MPPT structure. This choice helps to improve the performance of the closed-loop control under the fast varying irradiance conditions.

Since the DC-source voltage is full of switching noise, LPF is used to alleviate the effects of the noise. In this MPPT algorithm the signals V_{DC} and I_{DC} are sensed as inputs and the power P_{PV} is calculated. $V_{perturb}$ is the final perturbation in the reference voltage signal. At every switching instant, the signals V_{DC} and P_{PV} are band pass filtered to get the sinusoidal signals and LPF is used to remove the switching noise. After dividing this signal by Δu^2 signal to get $\partial p/\partial v$, the sign of this residue function is checked to get information about the operating point to see if it needs to move toward or away from MPP. K is a factor to control the speed of convergence. Finally, the results integrated to get the perturbation in the voltage reference.

The quantity sign ($\varepsilon_r = \partial p/\partial v$) is a clear indication of the region where the PV panel needs to operate as shown in Fig. 11.

- $((\varepsilon_r) > 0)$ means $p\sim$ and $v\sim$ are in phase and the operating point is at the left side of the MPP on the $(I-V)$ characteristic curve.
- $((\varepsilon_r) < 0)$ means $p\sim$ and $v\sim$ are out of phase and the operating point is at the right side of the MPP on the $I-V$ characteristic curve.

The knowledge of the instantaneous operating point makes it possible to change the PV voltage reference in order to approach the MPP. $\varepsilon_r = 0$ when the operating point reaches the MPP.

TABLE I
SPECIFICATION OF THE SINGLE PHASE GRID CONNECTED PV SYSTEM

Designator	Parameters	Unit
P_o	Rated power	$5kW$
f_{sw}	Switching frequency	$10kHz$
t_d	Dead time	$1.0\mu s$
L_i	Inverter side inductor	$1.5mH$
L_g	Grid side inductor	$0.75mH$
C_f	Filter capacitor	$6.0\mu F$
R_f	Damping resistor	$3.0\ \Omega$
V_g	Grid voltage	$220\,V$
f_g	Grid frequency	$60Hz$
$V_{DC-link}$	DC link voltage	$400\,V$

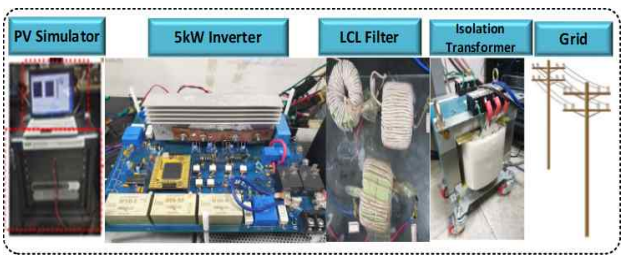

Fig. 12. Experimental setup.

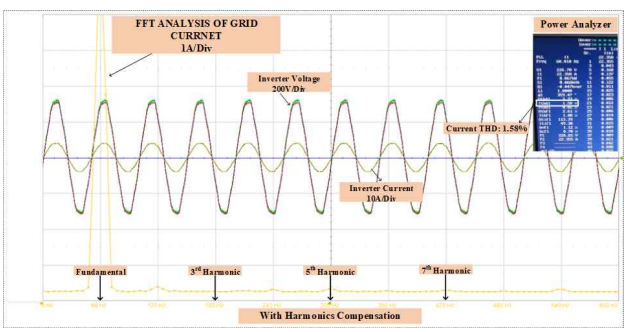

(a)

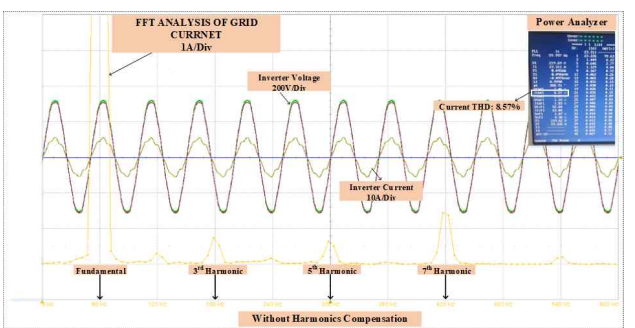

(b)

Fig. 13. Experimental results with a single phase GCI at 5 kW. (a) Inverter outputs without the proposed harmonic compensation method, (b) Inverter outputs with the proposed harmonic compensation method.

6. Experimental Result & Discussions

For the experimental verification of the proposed harmonic compensation technique with RCC- MPPT control, a prototype single phase GCI is built and connected to the $220V_{rms}$ grid through an LCL filter as shown in Fig. 12.

To verify the feasibility and validity of the proposed method, a 5kW inverter has been built. Experimental setup is shown in Fig. 13. TeraSAS ETS(600/17) Photovoltaic simulator has been used as a PV Source.

The control schemes are implemented in a Digital Signal Processor, DSP TMS320F28335 from Texas Instruments. In order to show the effectiveness of proposed method experiments are performed with and without the proposed DLA based harmonics elimination technique under the real grid condition. Fig. 13(a) shows the inverter outputs without the proposed DLA based harmonics elimination loop at 5kW. The four waveforms in each figure represent V_g, V_{in}, I_g and FFT analysis of grid current, respectively.

It can be observed from the FFT analysis in Fig. 13(a) that the 3rd and 5th and 7th harmonic are 1.449A, 0.645A, 1.129A, respectively, and the output current THD is 8.57%, which exceeds the value suggested by the IEEE Std. 519 and P-1547.

Fig. 13(b) shows the experimental results with the proposed DLA based harmonic compensation technique. It can be observed that the THD of the inverter current is significantly reduced from 8.57% to 1.58% at 5kW. The reductions of the 3^{rd} and 5^{th} harmonic and 7^{th} at 5kW are from 1.449A to 0.043A and from 0.645 to 0.158 and from 1.129 to 0.137, respectively. It can be confirmed by the experimental results that the proposed harmonic compensation method is very effective in compensating the harmonics at the CGI output.

Fig. 14 shows the performance of the PV system with the RCC MPPT strategy. Fig. 14(a) shows the MPPT trajectories captured on the P-V and I-V curves. As shown in the Fig. 14(a) the system is well tracking the MPP. The variation at MPP is negligible and MPPT efficiency is higher than 99.2% which demonstrate the stable MPP is achieved by the RCC-method. Fig. 14(b) shows the steady-state and dynamic performance of the MPPT by the PV source

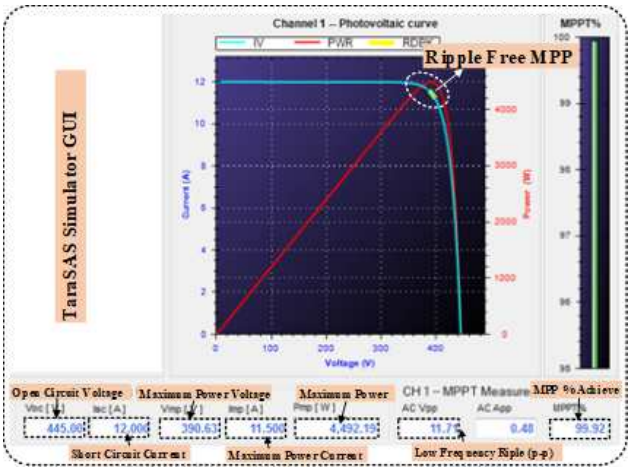

(a)

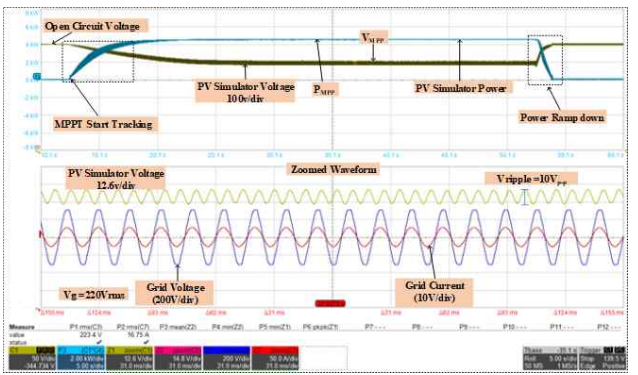

(b)

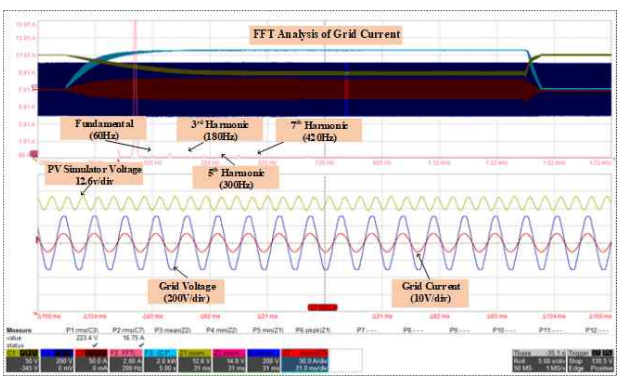

(c)

Fig. 14. (a) TeraSAS I-V/P-V curve, (b) Experimental results with MPPT, (c) Harmonic compensation results with MPPT and grid current FFT results.

and inverter waveforms. It is shown that the PV simulator voltage starts to decrease from V_{OC} and reach V_{mpp} and the inverter power increases smoothly at the same time. Fig 14(c) shows the performance of the harmonic compensation while achieving the MPPT operation.

Fig. 15 shows the performance of conventional and proposed DLA harmonic compensation method in terms of THD at different loads. It is clear that the proposed method shows an outstanding performance.

Fig. 15. Comparison of the inverter output THD with and without harmonic compensation method.

7. Conclusion

In this paper a novel inverter current harmonic elimination method by using DLA has been proposed and its validity has been proved by the experiments with a 5kW single phase GCI with RCC MPPT control. The proposed DLA based Harmonics compensation technique works with the principle of frequency shifting/demodulation and the amplitude and phase information of any n^{th} order harmonic can be extracted accurately under the highly distorted grid condition. The extracted harmonics are then subtracted from the output of the fundamental current controller to compensate for the harmonics. THD value of 1.58% has been achieved with the proposed method at 5kW while the MPPT efficiency is 99.2%.

References

[1] B. K. Bose, "Global warming: Energy, environmental pollution, and the impact of power electronics," *IEEE Industrial Electronics Magazine*, Vol. 4, No. 1, pp. 6-17, Mar. 2010.

[2] R. Teodorescu, F. Blaabjerg, M. Liserre, and P. C. Loh, "Proportional resonant controllers and filters for grid-connected voltage-source converters," in *Proc. Inst. Elect. Eng.-Electr. Power Appl.*, Vol. 153, No. 5, pp. 750-762, Sep. 2006.

[3] G. Shen, X. Zhu, J. Zhang, and D. Xu, "A new feedback method for PR current control of LCL-filter based grid-connected inverter," *IEEE Trans. Ind. Electron.*, Vol. 57, No. 6, pp. 2033-2041, Jun. 2010.

[4] M. Liserre, F. Blaabjerg, and S. Hansen, "Design and

control of an LCL-filter-based three-phase active rectifier," *IEEE Trans. Ind. Appl.*, Vol. 41, No. 5, pp. 1281-1291, Sep./Oct. 2005.
[5] M. Lisrerre, R. Teodorescu, and F. Blaabjerg, "Multiple harmonic control for three phase grid converter system with the use of PI-RES current controller in rotating frame," *IEEE Trans. Power Electronics*, Vol. 21, No. 3, May 2006.
[6] N. R. Zargari and G. Joos, "Performance investigation of a current-controlled voltage-regulated PWM rectifier in rotating and stationary frames," *IEEE Transactions on Industrial Electronics*, Vol. 42, No. 4, pp. 396-401, Aug. 1995.
[7] X. Liang and C. Andalib-Bin-Karim, "Harmonics and mitigation techniques through advanced control in grid-connected renewable energy sources: A review," *IEEE Transactions on Industry Applications*, Vol. 54, No. 4, pp. 3100-3111, Jul./Aug. 2018.
[8] IEEE, "IEEE draft standard for microwave filter definitions—Corrigendum 1," *IEEE P1549-2015/Cor1/D2*, pp. 1-11, Jan. 2016.
[9] M. Lisrerre, R. Teodorescu, and F. Blaabjerg, "Multiple harmonic control for three phase grid converter system with the use of PI-RES current controller in rotating frame," *IEEE Trans. Power Electronics*, Vol. 21, No. 3, May 2006.
[10] D. Sha, D. Wu, and X. Liao "Analysis of a hybrid controlled three phase grid-connected inverter with harmonic compensation in synchronous reference frame," *IET Power Electronic.*, Vol. 4, pp. 743-751, Sep. 2010.
[11] E. S. Kim, U. S. Seong, J. S. Lee, and S. H. Hwang, "Compensation of dead time effects in grid-tie single phase inverter using SOGI," in *Applied Power Electronic Conference and Exposition (APEC)*, pp. 2633-2637, 2017.
[12] A. G. Yepes, F. D. Freijedo, J. Doval-Gandoy, O. Lopez, J. Malvar, and P. Fernandez-Comesana, "Effect of discretization methods on the performance of resonant controllers," *IEEE Trans. Power Electronics*, Vol. 25, No. 7, pp. 1692-1712, Jul. 2010.
[13] A. G. Yepes, F. D. Freijedo, O. Lopez, and J. Doval-Gandoy, "High-performance digital resonant controllers implemented with two integrators," *IEEE Trans. Power Electronics*, Vol. 26, No. 2, pp. 1692-1712, pp. 563-576 Feb. 2011.
[14] M. Ciobotaru, R. Teodorescu, and F. Blaabjerg, "A new singlephase PLL structure based on second order generalized integrator," in *Proc. 37th IEEE Power Electronics Specialists Conference*, pp 1-6, 2006.
[15] A. Yazdani and R. Iravani, *Voltage-sourced converters in power systems: modeling, control, and applications. hoboken*, New Jersey: Wiley, pp. 451, 2010.

Saghir Amin

He was born in Mansehra, KPK, Pakistan in 1992. He received the B.E. degree in Electronics engineering from PAF-Karachi Institute of Economics & Technology, Karachi, Pakistan, in 2015. He received the M.S. degrees in electrical engineering from the Soongsil University, Seoul, Korea, in 2019. He is currently serving as Assistant Manager at HnPower.Inc.Ltd Daejeon, South Korea.

Muhammad Noman Ashraf

He was born in Karachi, Pakistan in 1993. He received his M.S. degree in Electrical Engineering from, Soongsil University Seoul, South Korea. He became the recipient of a scholarship from the Soongsil University and joined the Department of Electrical Engineering as Research Assistant in 2017 for two years. Currently, He is full time Research Engineer in the industrial company i.e. OKY LTD, in Seoul.

Woojin Choi

He was born in Seoul, South Korea, in 1967. He received the B.S. and M.S. degrees from Soongsil University, Seoul, in 1990 and 1995, respectively, and the Ph.D. degree from Texas A&M University, College Station, TX, USA, in 2004, all in electrical engineering. From 1995 to 1998, he was a Research Engineer with the Central Research and Development Division, Daewoo Heavy Industries. In 2005, he joined the School of Electrical Engineering, Soongsil University, Seoul. He is an Associate Editor of IEEE Transactions on Industry Applications.